Development of a Data Assimilation Method Using Vibration Equation for Large - Eddy Simulations of Turbulent Boundary Layer Flows

AUTHOR(S):

Nakayama, Hiromasa; Takemi, Tetsuya

CITATION:

Nakayama, Hiromasa ...[et al]. Development of a Data Assimilation Method Using Vibration Equation for Large - Eddy Simulations of Turbulent Boundary Layer Flows. Journal of Advances in Modeling Earth Systems 2020, 12(8): e2019MS001872.

ISSUE DATE:

2020-08

URL:

http://hdl.handle.net/2433/253553

JAMES | Journal of Advances in Modeling Earth Systems

RESEARCH ARTICLE
10.1029/2019MS001872

Key Points:
- A data assimilation method using a vibration equation for large-eddy simulations of turbulent boundary layer flows was developed
- The natural frequency in the vibration equation was set to be smaller than the spectral peak frequency in the background turbulence
- The data assimilation using the vibration equation successfully nudges toward the target mean winds while maintaining small-scale turbulent fluctuations well

Correspondence to:
H. Nakayama,
nakayama.hiromasa@jaea.go.jp

Citation:
Nakayama, H., &Takemi, T. (2020). Development of a Data Assimilation Method Using Vibration Equation for Large-Eddy Simulations of Turbulent Boundary Layer Flows. *Journal of Advances in Modeling Earth Systems*, *12*, e2019MS001872. https://doi.org/10.1029/2019MS001872

Received 27 AUG 2019
Accepted 20 MAY 2020
Accepted article online 19 JUN 2020

Development of a Data Assimilation Method Using Vibration Equation for Large-Eddy Simulations of Turbulent Boundary Layer Flows

Hiromasa Nakayama[1] and **Tetsuya Takemi**[2]

[1]Japan Atomic Energy Agency, Ibaraki, Japan, [2]Disaster Prevention Research Institute, Kyoto University, Kyoto, Japan

Abstract In order to improve the simulation accuracy, it is effective to use a data assimilation technique which is capable of reproducing more realistic simulated states by incorporating observational data into simulation models. One of the simplest ones among data assimilation techniques is a Newtonian relaxation-type nudging method which has been widely used in mesoscale meteorological models. In this study, we proposed a data assimilation method using a vibration equation which can incorporate turbulence winds toward target mean winds while maintaining small-scale turbulent fluctuations as a different approach from the conventional nudging method. First, we conducted test simulations in which nudging is applied in a basic turbulent boundary layer (TBL) flow toward a target one. It is shown that the basic TBL flow can be reasonably nudged toward the target one while maintaining the turbulent fluctuations well when prescribing the natural frequency in the vibration equation smaller than the spectral peak frequency in the TBL flow. Then, we applied the proposed nudging method by incorporating data obtained from meteorological observations located in the actual city of Kyoto. The mean wind velocity profiles were reasonably nudged toward the target observed profile and the turbulence statistics were also favorably maintained. It is concluded that the data assimilation method using the vibration equation successfully nudges toward the target mean winds while maintaining small-scale turbulent fluctuations well.

Plain Language Summary In order to improve the simulation accuracy, it is effective to use a data assimilation technique which is capable of reproducing more realistic simulated states by incorporating observational data into simulation models. Since the observational data assimilated are normally averaged in time and/or in space by filtering out small-scale turbulent fluctuations, the conventional data assimilation method is not suitable for large-eddy simulations of unsteady turbulent flows. In this study, we proposed a data assimilation method using a vibration equation which can nudge turbulence winds toward target mean winds while maintaining small-scale turbulent fluctuations. It was shown that our proposed method is capable of both nudging the flow fields toward a target state and retaining the fluctuating nature of turbulent flows. The data assimilation method using a vibration equation is suitable for LES models and has a high potential to practically reproduce more realistic atmospheric state.

1. Introduction

Air quality in urban environments is directly influenced by mainly two factors: atmospheric thermal stability and surface roughness. In terms of thermal stability, the atmospheric state is governed by the changes of weather systems at various spatial scales and also determined by the diurnal variability of solar forcing. During the daytime, the ground surface is heated by solar radiation, and turbulence is mainly produced by positive buoyancy, which induces boundary layer convective motions. This type of the atmospheric boundary layer (ABL) is called as convective boundary layer (CBL). During the night, the ground surface is cooled by outgoing long-wave radiation, and turbulence is constrained by negative buoyancy, which forces turbulent motions more inactive and leads to stable stratification. This type is called as stable boundary layer (SBL). In terms of surface roughness, the boundary layer over a rough surface can be characterized into roughness sublayer (RS) and the inertial sublayer (IS). In the RS, the strong three-dimensionality of turbulent flows is observed and the flow patterns are directly determined by the building morphological characteristics. The IS ranges up to 2 to 5 times the height of the buildings. In the RS above the IS, the vertical variation of the shear stress may be neglected and the wind direction is assumed to be constant with

height. However, it was pointed out that the IS may not exist at all in some of extremely rough urban areas (Cheng & Castro, 2002).

For investigating air quality in complex urban environments, a computational fluid dynamics (CFD) technique is helpful. In particular, the CFD simulations based on large-eddy simulation (LES) model have come to be regarded as an effective prediction method for environmental flows and can provide detailed information on turbulence structures and mean and fluctuating concentrations of a plume. However, simulation results are highly sensitive to input conditions, modeling of subgrid scale (SGS) turbulent eddies, and grid resolution. Specifically, input conditions are imposed by field measurements or operational meteorological observations. For example, Warner et al. (2004) investigated the influence of the input conditions on the performance of the model predictions for mean concentrations of a plume released within urban environments using meteorological observations obtained at different locations. They reported that the model inputs that included meteorological information close to the plume source led to the worst performance because the meteorological measurements might have had significant variability induced by the urban buildings. This implies that it is difficult to ensure the representativeness of the observations at a stationary point to be assimilated into turbulent flows and plume dispersion in the complex urban environments. Nakayama et al. (2016) conducted LESs of plume dispersion in the urban central district of Oklahoma City under realistic atmospheric conditions during the field campaign Joint Urban 2003 by coupling the LES model with a mesoscale meteorological simulation (MMS) model and concluded that the prediction accuracy of the high-resolution simulations highly depends on the quality and reproducibility of the wind speed and direction simulated by the mesoscale model against the observed data during the field experiments.

SGS modeling is also critically important. Iizuka and Kondo (2004) evaluated the performance of various SGS models under a neutral condition and showed that there is a tendency of overestimation of wind speeds near the ground surface by the dynamic SGS model (Germano et al., 1991) in comparison with the conventional static SGS model (Smagorinsky, 1963). On the other hand, it was shown from the intercomparison of LESs for the SBL flows that the static Smagorinsky model at a coarse grid resolution is not able to sufficiently represent a pronounced supergeostrophic jet peaking near the top of the boundary layer in comparison with the sophisticated SGS models (Beare et al., 2006).

As for a grid resolution issue, according to sensitivity analyses of grid resolution by Santiago et al. (2008) and Xie and Castro (2006), each building should be resolved by at least 15–20 grid points for each direction in order to accurately capture turbulent flows around individual buildings. Kanda (2006) also mentioned that 10 grid points for each building dimension induce underestimation of the turbulent statistical values within the building height. However, it is practically difficult to explicitly resolve all the buildings in urban areas at 15–20 grid points, because of computational costs. Therefore, simulation results always include more or less calculation errors.

In order to improve the simulation accuracy, it is effective to use a data assimilation technique which is capable of reproducing more realistic simulated states by incorporating observational data into simulation models. One of the simplest ones among data assimilation techniques is a Newtonian relaxation-type nudging method in the following expression:

$$\left.\frac{\partial \varphi}{\partial t}\right|_{\mathrm{NUD}} = -\frac{[\varphi] - \varphi_{\mathrm{target}}}{\tau} \tag{1}$$

Here, φ is a variable such as wind velocities, temperature, and concentration. $[\varphi]$ is a spatially or temporally averaged variable over the simulated domain, and $\varphi_{\mathrm{target}}$ is a target value. t and τ are time and a relaxation timescale, respectively. This type of nudging method has been widely used in mesoscale meteorological models such as Mesoscale Model Version 5 (MM5) (Dudhia, 1993), the Weather Research and Forecasting (WRF) model (Skamarock et al., 2008), and others. Such a nudging method is also used in LES models (e.g., the Parallelized Large-Eddy Simulation Model [PALM] developed by Maronga et al., 2015).

Here, a serious issue is encountered when nudging is applied toward target mean winds by the conventional nudging method in LES models. Since $\varphi_{\mathrm{target}}$ is usually given by the meteorological observed (OBS) data which are temporally averaged in 10-min to 1-h intervals and do not include small-scale turbulent

fluctuations, the fluctuating components of wind velocities are accordingly damped when prescribing the larger relaxation timescale to match with the target mean winds. In contrast, when prescribing the smaller one to maintain the fluctuating components, the background mean winds are poorly nudged toward the target ones. Maronga et al. (2015) mentioned that τ should be chosen large enough on the order of several hours to allow an undisturbed development of the small-scale turbulence in the LES model and should be chosen small enough to account for synoptic disturbances based on the discussion on the trade-off between turbulence and large-scale disturbances by Neggers et al. (2012). Heinze et al. (2017) also mentioned that $\tau = 6$ h is long enough for the fast boundary layer physics to develop their own unique state and short enough so that larger-scale disturbances such as weather fronts in the LES.

In this study, we propose a data assimilation method using a vibration equation which can nudge turbulence winds toward target mean winds while maintaining small-scale turbulent fluctuations as a different approach from the Newtonian relaxation-type nudging method. First, we conduct test simulations in which nudging is applied in a basic turbulent boundary layer (TBL) flow toward a target one. Then, we apply the proposed nudging method by incorporating data obtained from meteorological observations located in the southern part of the actual city of Kyoto and evaluate our proposed method by comparing the data-assimilated LES results with the empirical formulas and experimental data.

2. Formulation of the Data Assimilation Using Vibration Equation

We propose here a data assimilation method using a vibration equation in order to nudge the LES-generated turbulence winds toward the target mean winds while maintaining the turbulent fluctuations. The spatially filtered continuity and Navier-Stokes (N-S) equations are as follows:

$$\frac{\partial \overline{u}_i}{\partial x_i} = 0 \tag{2}$$

$$\frac{\partial \overline{u}_i}{\partial t} + \overline{u}_j \frac{\partial \overline{u}_i}{\partial x_j} = -\frac{1}{\rho}\frac{\partial \overline{p}}{\partial x_j} - \frac{\partial}{\partial x_j}\tau_{ij} - \mathrm{damp}(x) f_i + f_c\left(\overline{u}_2 - V_g\right)\delta_{i1} - f_c\left(\overline{u}_1 - U_g\right)\delta_{i2} \tag{3}$$

where u_i, p, ρ, τ_{ij}, f_i, f_c, U_g, and V_g are the wind velocity, pressure, density, SGS Reynolds stress, the nudging term, Coriolis parameter, and the horizontal components of the geostrophic wind, respectively. Subscripts i and j stand for coordinates (streamwise direction, $x_1 = x$; spanwise, $x_2 = y$; and vertical, $x_3 = z$). Overbars indicate that the variable is spatially filtered. damp(x) is a damping function for the streamwise direction. δ_{ij} is the Kronecker delta ($\delta_{ij} = 1$ for $i = j$, 0 otherwise). The vibration equation for the velocity oscillating around a zero-wind basic state with a certain frequency is as follows:

$$\frac{d^2\overline{u}_i}{dt^2} + \gamma\frac{d\overline{u}_i}{dt} + \omega_0^2\overline{u}_i = 0 \tag{4}$$

where γ and ω_0 are the damping constant and natural frequency, respectively. The second and third terms are the damping and oscillating terms, respectively. When integrating Equation 4 in time, the following equation is derived.

$$f_i = -\rho\frac{d\overline{u}_i}{dt} = \rho\gamma\overline{u}_i + \rho\omega_0^2\int_0^t \overline{u}_i dt' \tag{5}$$

If we assume here that there is a target mean wind condition as a basic state around which vibrate motion occurs, non-zero winds appear on the right-hand side of Equation 5. Here the target mean winds are assumed to be observed winds (denoted as U_{OBS}), and hence, the following equation is derived.

$$f_i(x, y, z, t) = \rho\gamma\left(\overline{u}_i(x, y, z, t) - U_{i,\mathrm{OBS}}(z, t)\right) + \rho\omega_0^2\int_0^t \left(\overline{u}_i(x, y, z, t') - U_{i,\mathrm{OBS}}(z, t')\right)dt' \tag{6}$$

In the right-hand side, the first term is the damping term and the second term is the oscillating term. The damping term here is the one conventionally used to nudge the simulated fields toward targeted observed winds (typically mean winds, see Equation 1) and γ corresponds to τ^{-1}.

This formulation is similar to that of a proportional and integral (PI) controlled forcing method originally proposed by Spille-Kohoff and KaltenBach (2001). The PI method adds the forcing term to the wall-normal momentum equation that amplifies the velocity fluctuations in that direction, thus enhancing the production term in the shear stress budget. In their study, the PI terms were given by the error of the Reynolds shear stress between the Reynolds-averaged N-S (RANS) and LES. The PI terms in the PI method correspond to the damping and oscillating terms in the right-hand side of Equation 6, respectively. The former term plays a role in determining the forcing amplitude based on the error in the Reynolds shear stress. The latter also plays an important role in reducing the response to very sharp changes which could induce a numerical instability by the time-dependent restoring force. Keating et al. (2006) and Laraufie et al. (2011) successfully generated unsteady turbulent inflow conditions for LESs from a steady state of a RANS by hybrid RANS/LES simulations in which an LES region is appended to a RANS one, and the RANS statistical results (mean velocity and Reynolds shear stress) are used to prescribe the LES inflow conditions.

Because the oscillating term has a property of fluctuating around the target mean values by the action of the time-dependent restoring force, it can be recognized as one of the effective nudging methods. Therefore, we focus only on the oscillating term to nudge toward the target fields by utilizing the property while maintaining wind velocity fluctuations. The following equation is thus derived.

$$f_i(x, y, z, t) = \rho\omega_0^2 \int_0^t \left(\overline{u}_i(x, y, z, t') - U_{i,\mathrm{OBS}}(z, t')\right)dt' \tag{7}$$

Equation 7 is the nudging term and is incorporated into the N-S equation 3.

3. Computational Model and Settings

The CFD model used here is local-scale high-resolution atmospheric dispersion model using LES (LOHDIM-LES) developed by Nakayama et al. (2012, 2014, 2016). The governing equations are the filtered continuity equation and the filtered N-S equation. The SGS effects are represented by the standard Smagorinsky model (Smagorinsky, 1963) with a constant of 0.1. The coupling algorithm of the velocity and pressure fields is based on the marker-and-cell method (Harlow & Welch, 1965) with the second-order Adams-Bashforth scheme for time integration. The Poisson equation is solved by the successive overrelaxation method. A second-order accurate central difference scheme is used for the spatial discretization in the basic equations.

In this study, two computational regions are set up as shown in Figure 1. One is the driver region for generating a basic TBL flow 0.14 driven by a constant pressure gradient $-u_*^2/H$, and the other is the analysis region for nudging toward the target one. In this region, the pressure gradient term is excluded and the Coriolis forcing term is incorporated to keep the TBL flow. u_* and H are the friction velocity and the height of the computational domain, respectively. In the driver region, a periodic condition is imposed for the streamwise direction and the Monin-Obukhov similarity theory (Monin & Obukhov, 1954) is applied at the bottom surface.

$$\tau_{i3\_\mathrm{bottom}} = -\left(\frac{\kappa\overline{u}_i}{ln(z/z_0)}\right)^2 \tag{8}$$

κ and z_0 are the von Karman constant and roughness length, respectively. At the top, free-slip conditions for streamwise and spanwise velocity components are imposed and the vertical velocity component is 0. In the analysis region, at the exit boundary, a zero-gradient condition is applied and other boundary conditions at the top, bottom, and side are the same as the driver region. At the inlet, the wind velocity data obtained at the driver region are imposed at the inlet of the analysis region at every time step. The size and grid resolution of the two computational regions are $6{,}000 \times 6{,}000 \times 1{,}000$ and $40 \times 40 \times 10$ m in the streamwise, spanwise, and vertical directions, respectively.

The bell-shaped damping function shown in Figure 2 is set to smoothly nudge toward the target data as the following expression:

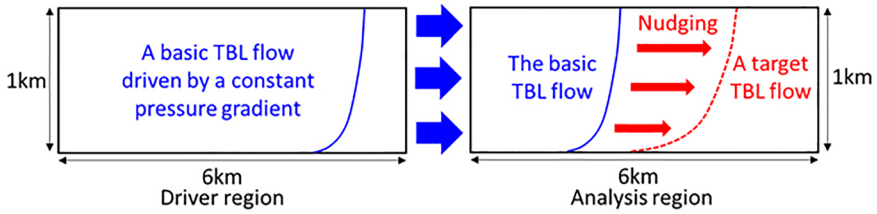

Figure 1. Computational model.

$$\mathrm{damp}(x) = -\sin^2\left[\frac{\pi}{2}\left(1 - \frac{x_{\mathrm{nud}} - x}{x_l}\right)\right] \tag{9}$$

Here, x_{nud} and x_l are the downstream position where the target data are inputted and the length of the damping layer for the streamwise direction, respectively. The shape of this function is typically used for the WRF model in order to smoothly relax. Those values were set to 3 km and 500 m, respectively. In a local scale of several kilometers, atmospheric conditions can be nearly homogeneous in the horizontal direction. Kanda et al. (2013) conducted LESs of fully developed TBL flows within and above explicitly resolved buildings in actual urban central districts in Japan and made a data set of the horizontally averaged turbulent statistics and surface drag evaluated over 1 × 1 km areas corresponding to the urban morphologies. They mentioned that the vertical profiles of horizontally averaged wind velocity mostly follow a logarithmic law even for districts with high-rise buildings. This fact ensures that the representative horizontal scale of TBL flows is 1 km. In order to nudge the target observed winds obtained at a stationary point, the nudging area was set to have a length of 1 km and range from 2.5 to 3.5 km downstream positions from the inlet boundary.

4. Test Simulations

4.1. Setting Computational Cases

We first generated the basic TBL flow with a power law exponent $n = 0.14$ in the driver region by setting $z_0 = 0.1$ m and $u_* = 0.45$ m/s in Equation 8. Then, against this basic TBL flow, we imposed target streamwise mean winds approximated by the power law profile of $n = 0.25$ at 3 km downstream position from the inlet

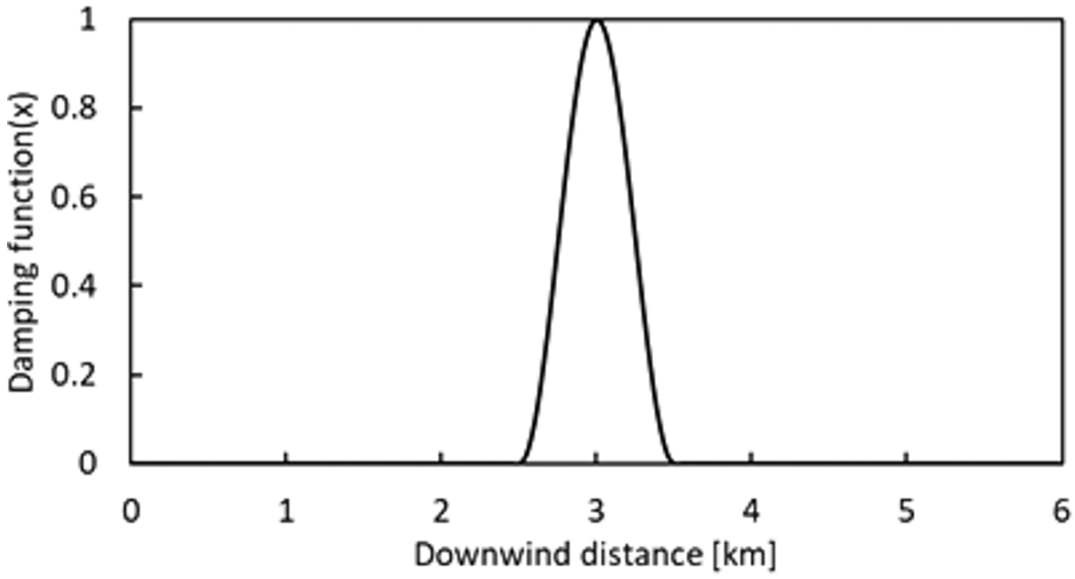

Figure 2. The damping function. 0 and 6 km indicate the inlet and outlet boundaries, respectively. The input data for data assimilation are located at the downstream position of 3 km.

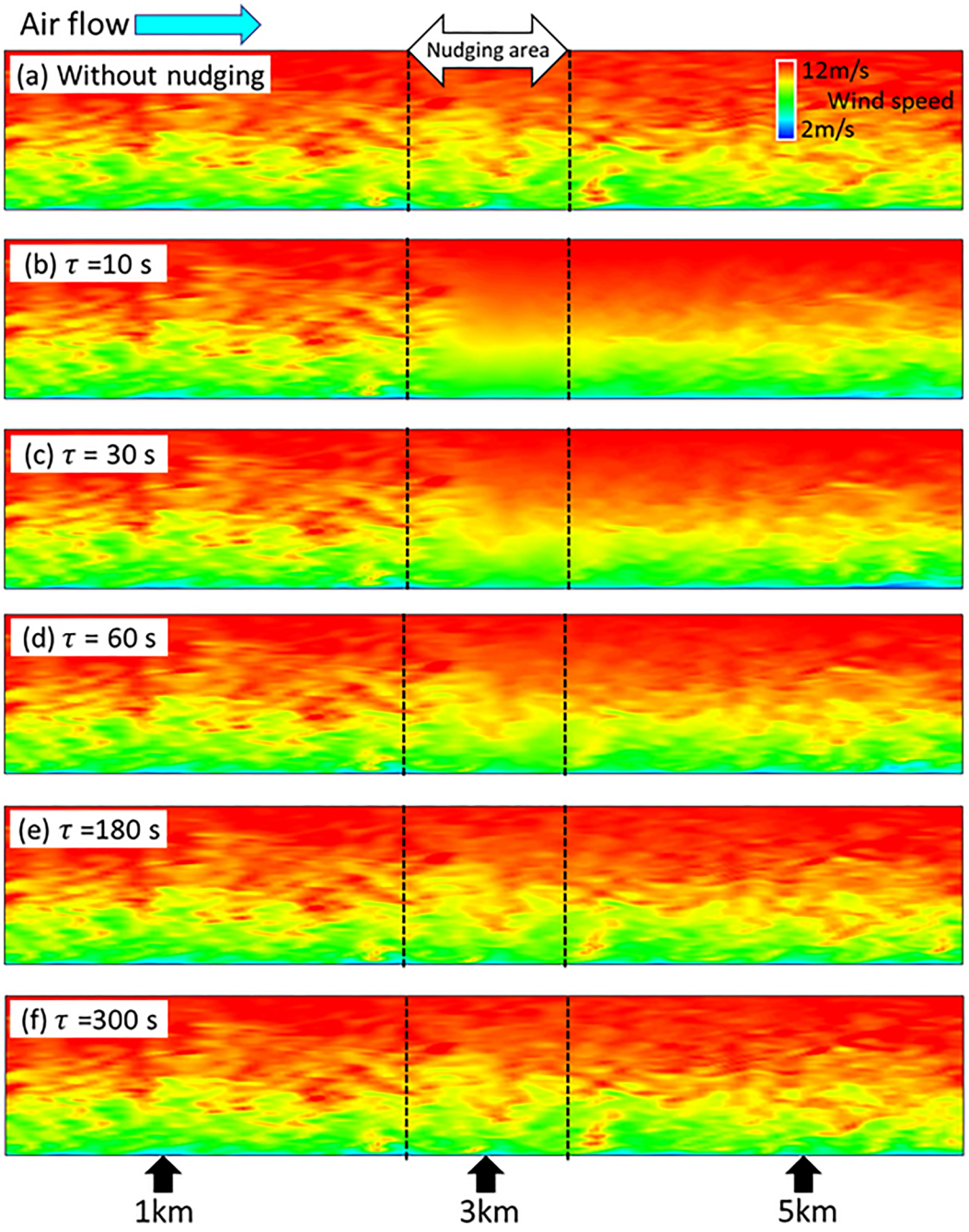

Figure 3. Instantaneous fields of wind speeds by the Newtonian relaxation-type nudging data assimilation method for the cases (a) without nudging, (b) $\tau = 10$ s, (c) $\tau = 30$ s, (d) $\tau = 60$ s, (e) $\tau = 180$ s, and (f) $\tau = 300$ s.

boundary in the analysis region. Note here that in the present test simulations, the target winds do not vary with time. The target mean winds for the spanwise and vertical components are 0. The turbulence characteristics obtained at the analysis region were calculated during a 30-min period after the flow reached an equilibrium state.

4.2. The Results of the Conventional Nudging Method

Figure 3 shows instantaneous wind fields by the conventional Newtonian relaxation-type nudging method in the analysis region. For cases (b) to (f), the relaxation timescale τ was set to 10, 30, 60, 180, and 300 s,

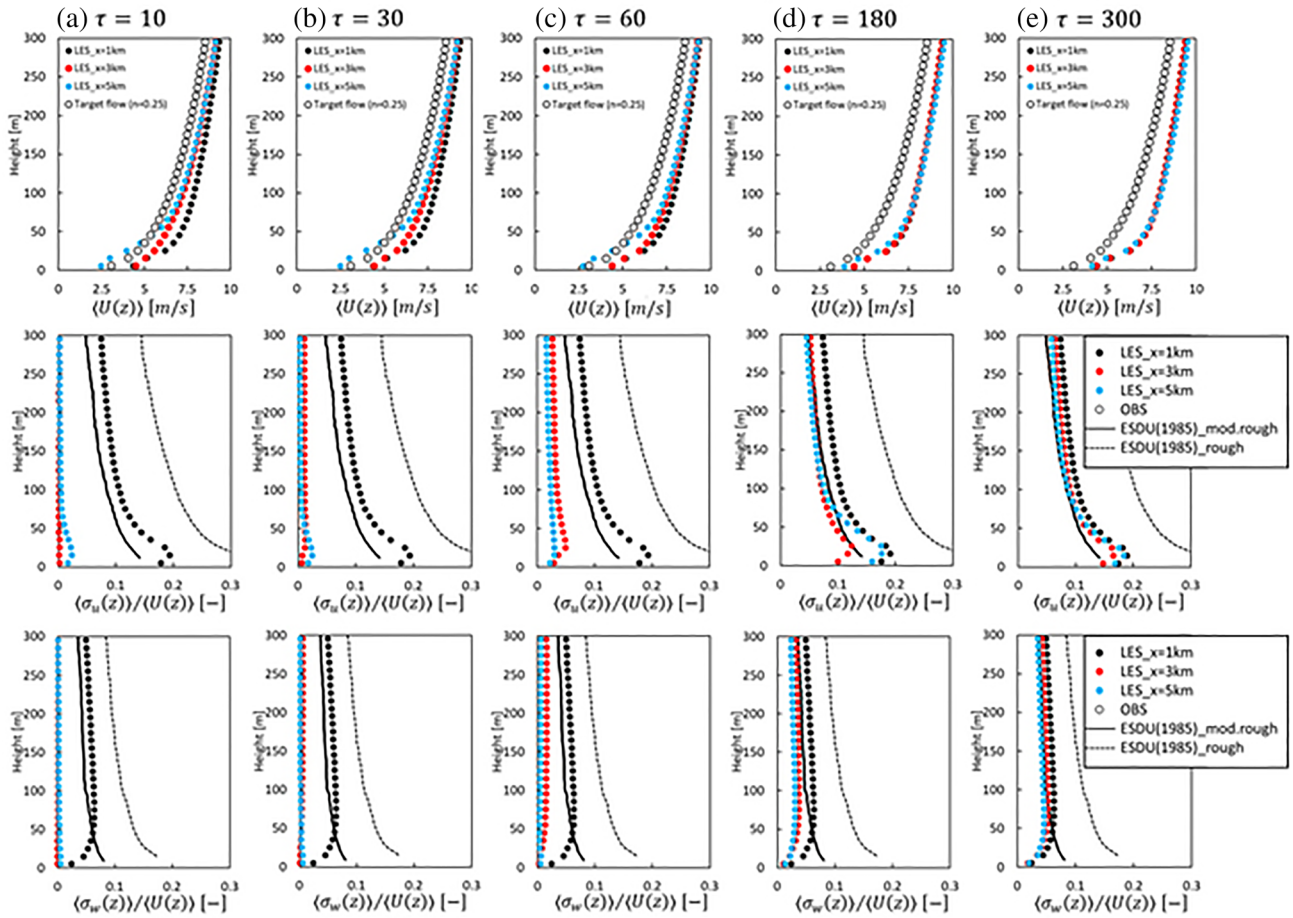

Figure 4. Vertical profiles of mean wind velocity (top), streamwise turbulence intensity (middle), and vertical turbulence intensity (bottom) for the cases of (b) $\tau = 10$ s, (c) $\tau = 30$ s, (d) $\tau = 60$ s, (e) $\tau = 180$ s, and (f) $\tau = 300$ s.

respectively. For cases (b) and (c) (i.e., $\tau = 10$ and 30 s), the turbulent fluctuations are found to be rapidly damped at downstream positions from the nudging area. For case (d) ($\tau = 60$ s), it seems that the turbulent motions are damped from the nudging area. For cases (e) and (f) ($\tau = 180$ and 300 s), the turbulent motions are maintained throughout the computational region and are similar to those for case (a) without nudging.

Figure 4 shows the vertical profiles of the 30-min averaged wind velocities $U(z)$ and the streamwise and vertical turbulence intensities $\sigma_u(z)$ and $\sigma_w(z)$ for each case. Here, the angled brackets denote a spatial average for the spanwise direction. The turbulence intensities are compared with the recommended data of Engineering Science Data Unit (ESDU) 85020. The ESDU provides comprehensive turbulence characteristics of a neutrally stratified ABL based on independent experimental measurements ranging from the ground surface to 300 m, including the vertical profiles of turbulence intensities and their relationships depending on surface roughness. For cases (b) and (c), the mean wind velocities become close to the target ones at the nudging area and match with them at $x = 5$ km. However, both turbulence intensities are rapidly damped at downstream positions from the nudging area. Especially for cases (e) and (f), it is found that those do not become close to the target ones and both turbulence intensities are damped a little. It is expected that the results are not significantly changed for cases of τ %3E 300 s.

Figure 5 shows the vertical profiles of the streamwise wind velocity budget at the nudging point. Each term is spatially averaged for the spanwise direction. Those are analyzed based on the following budget equation for the streamwise wind velocity shown by Dupont et al. (2011).

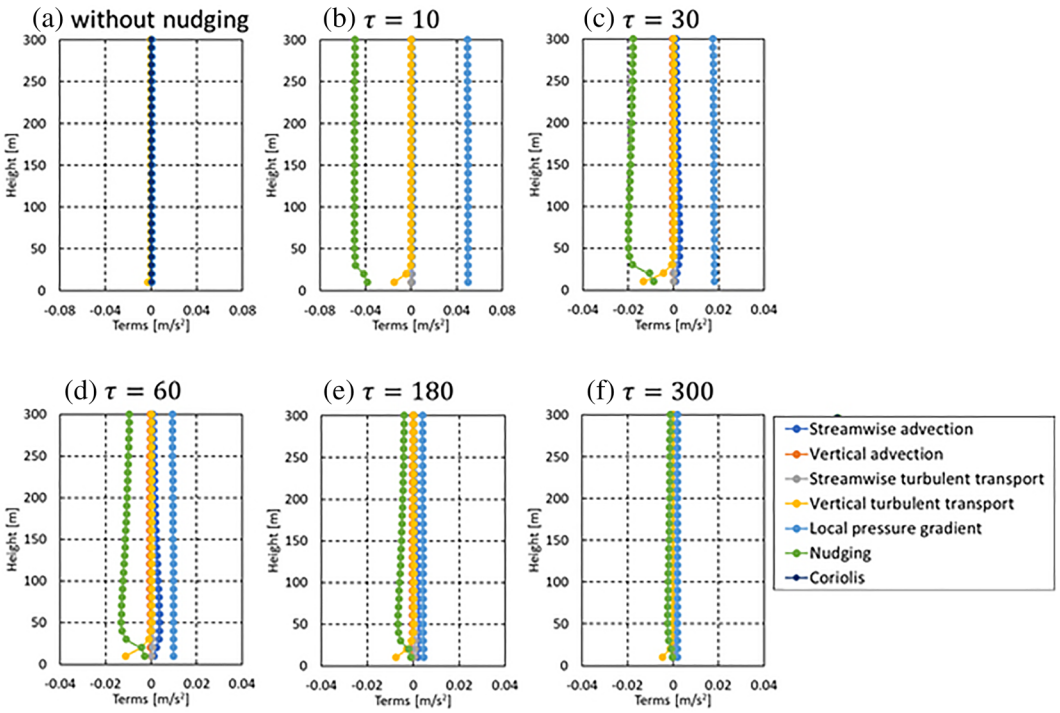

Figure 5. Vertical profiles of the streamwise wind velocity budgets at the nudging point of $x = 3$ km for the cases of (a) without nudging, (b) $\tau = 10$ s, (c) $\tau = 30$ s, (d) $\tau = 60$ s, (e) $\tau = 180$ s, and (f) $\tau = 300$ s.

$$\frac{\partial\langle u\rangle}{\partial t} = 0 = -\langle u\rangle\underbrace{\frac{\partial\langle u\rangle}{\partial x}}_{\text{(I)}} - \langle w\rangle\underbrace{\frac{\partial\langle u\rangle}{\partial z}}_{\text{(II)}} - \underbrace{\frac{\partial\langle u'u'\rangle}{\partial x} - \frac{1}{\rho}\frac{\partial\langle\tau_{11}\rangle}{\partial x}}_{\text{(III)}} - \underbrace{\frac{\partial\langle u'w'\rangle}{\partial z} - \frac{1}{\rho}\frac{\partial\langle\tau_{13}\rangle}{\partial z}}_{\text{(IV)}} - \underbrace{\frac{1}{\rho}\frac{\partial\langle p\rangle}{\partial x}}_{\text{(V)}} + \underbrace{f_c\left(\overline{u}_2 - V_g\right)}_{\text{(VI)}} - \underbrace{\text{damp}(x)f_1}_{\text{(VII)}} \tag{10}$$

The terms on the right-hand side represent the streamwise (I) and vertical (II) advection by the mean flow, streamwise (III) and vertical (IV) turbulent transport from both resolved scale and SGS, local pressure gradient (V), Coriolis force (VI), and nudging (VII). It is found that the streamwise momentum budget is dominated by local pressure gradient and nudging for cases (b) and (c) of $\tau = 10$ and 30 s, acting as a momentum source and sink, respectively. All other terms seem to be negligible. For case (f) of $\tau = 300$ s, the budget is still dominated by local pressure gradient and nudging although the vertical profile patterns are similar to those without nudging. The vertical profile of the vertical turbulent transport shows a negative peak near the ground surface because it is difficult to capture near-wall turbulent behaviors by the standard Smagorinsky model (Moin & Kim, 1982).

It seems that it is difficult to nudge toward the target mean winds while maintaining turbulent fluctuations under a condition of a range of short timescales (the order of 10 min) by the conventional Newtonian relaxation-type nudging method.

4.3. The Results of the Sensitivity Experiments by the Proposed Nudging Method

In the data assimilation method using the vibration equation, it is important to set an appropriate value for the natural angular frequency ω_0 in order not to damp turbulent fluctuations. In this study, we determined the value by conducting a number of sensitivity experiments. Figure 6 shows the power spectra of the basic TBL flows for the streamwise, spanwise, and vertical components at heights of 50, 100, and 200 m, respectively. Those were calculated during a 30-min period after the flow reached an equilibrium state. The spectral peak frequency f_{peak} at heights from 50 to 200 m lies in the range from 0.020 to 0.024 s^{-1}. Based on these

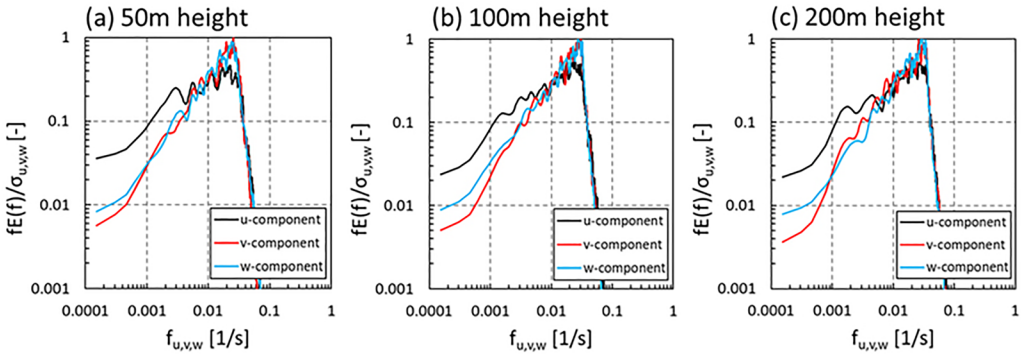

Figure 6. The power spectra for each component of the basic TBL flow in the driver region.

peak values, we set various natural frequency values in the vibration equation. The test simulation cases are listed in Table 1. The value was set to be constant for the vertical direction. Here, ω_0 in Equation 7 was given from $\omega_0 = 2\pi f_0$.

In data-assimilated LES results, the background mean winds should be close to the target one at the nudging area and the equilibrium state of the turbulence should also be maintained throughout the computational region. Here, we compare the vertical profile of mean velocity mainly with that of the target one at the nudging area and estimate the streamwise variation of the vertical profiles of turbulence intensities and Reynolds stresses. Figure 7 shows instantaneous wind fields by assimilating the target mean winds for each case. For cases (a) and (b) (i.e., f_0 %3E f_{peak}), the turbulent fluctuations are found to be rapidly damped at downstream positions from the nudging area. For case (c) ($f_0 \fallingdotseq f_{peak}$), it seems that the turbulent motions are maintained throughout the computational region. For cases (d) and (e) (f_0 %3C f_{peak}), the turbulent motions are active and are maintained throughout the computational region.

Figure 8 shows the vertical profiles of the mean wind velocities for each case. For cases (a) and (b) of f_0 %3E f_{peak}, the mean wind velocity profile matches with the target one at the nudging area of $x = 3$ km. For case (c) of $f_0 \fallingdotseq f_{peak}$, that becomes similar to the target one at the nudging area. For cases (d) and (e) of f_0 %3C f_{peak}, that becomes close to the target one at the nudging area. However, the mean wind velocity profile at a downwind position from the nudging area of $x = 5$ km returns to the original profile at $x = 1$ km. This tendency is different from that for cases (b) and (c) ($\tau \leq 30$ s) obtained by the conventional Newtonian relaxation-type nudging method as shown in Figure 4. The cause needs to be further investigated in the future.

Figures 9–11 compare the vertical profiles of the streamwise, spanwise, and vertical turbulence intensities with the ESDU recommended data. For cases (a) and (b) of f_0 %3E f_{peak}, three components of the turbulence intensities are rapidly decreased and become much smaller than the ESDU data for a moderately rough surface at downwind positions from the nudging area of $x \geq 3$ km. For case (c) of $f_0 \fallingdotseq f_{peak}$, the streamwise turbulence intensities are decreased and are smaller than the ESDU data for a moderately rough surface below 150-m height at $x = 3$ km although those recover at $x = 5$ km. The spanwise and vertical turbulence intensities are slightly decreased at $x \geq 3$ km. On the other hand, for cases (d) and (e) of f_0 %3C f_{peak}, the vertical profiles of each component of the turbulence intensities at each downstream position are similar to one another and lie in the range of the ESDU data except near the ground surface.

Table 1
Test Simulation Cases for Sensitivity Experiments

Test cases	f_{peak} of the basic TBL flow	f_0 set in the vibration equation
Case (a)	u-comp: 0.020–0.024 [1/s]	0.2 [1/s]
Case (b)		0.05 [1/s]
Case (c)	v-comp: 0.026–0.030 [1/s]	0.02 [1/s]
Case (d)	w-comp: 0.024–0.030 [1/s]	0.005[1/s]
Case (e)		0.002 [1/s]

Figure 12 shows the vertical profiles of the Reynolds stresses $\overline{u'w'}(z)$ for each case. The distribution patterns depending on the values of are the same as the turbulence intensities. For cases (a) and (b) of f_0 %3E f_{peak}, the Reynolds stresses are rapidly decreased at $x \geq 3$ km. For case (c) of $f_0 \fallingdotseq f_{peak}$, those are rapidly decreased at $x = 3$ km although those recover at $x = 5$ km. For cases (d) and (e) of f_0 %3C f_{peak}, those profiles are similar to one another at each

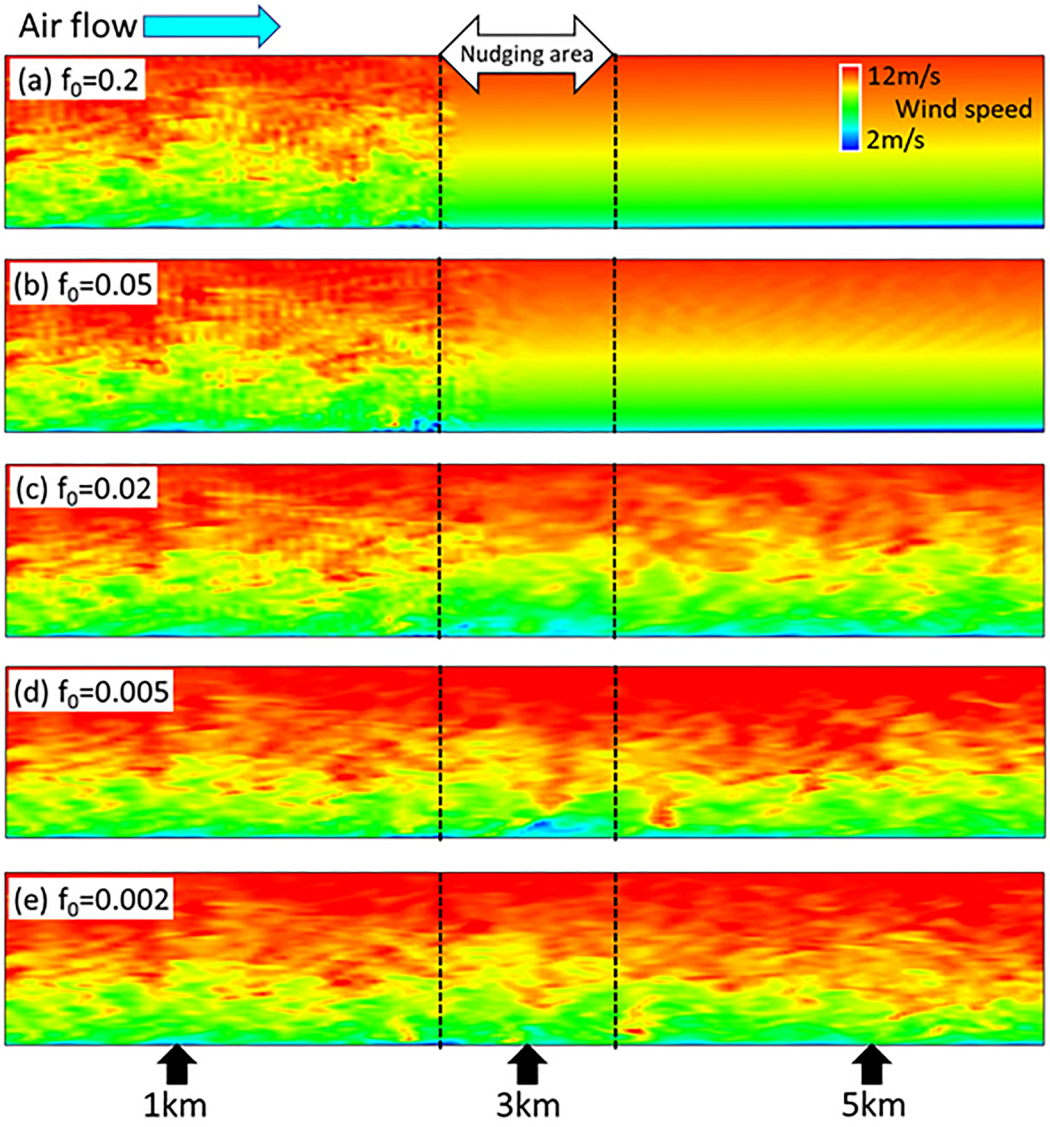

Figure 7. Instantaneous fields of wind speeds by the data assimilation method for the cases of (a) $f_0 = 0.2\ s^{-1}$, (b) $f_0 = 0.05\ s^{-1}$, (c) $f_0 = 0.02\ s^{-1}$, (d) $f_0 = 0.005\ s^{-1}$, and (e) $f_0 = 0.002\ s^{-1}$.

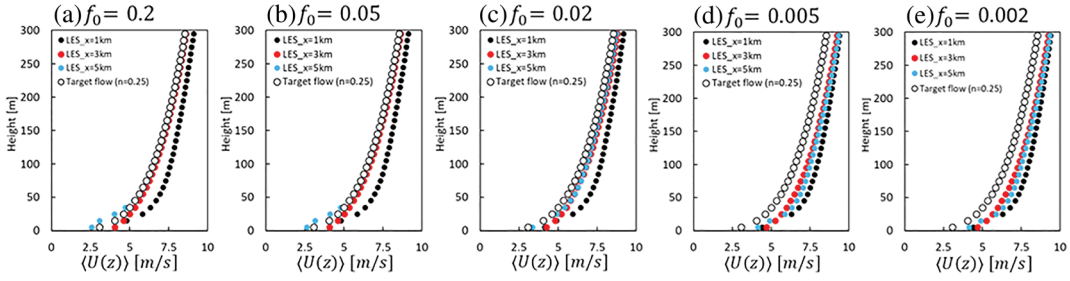

Figure 8. Vertical profiles of mean wind velocity for the cases of (a) $f_0 = 0.2\ s^{-1}$, (b) $f_0 = 0.05\ s^{-1}$, (c) $f_0 = 0.02\ s^{-1}$, (d) $f_0 = 0.005\ s^{-1}$, and (e) $f_0 = 0.002\ s^{-1}$.

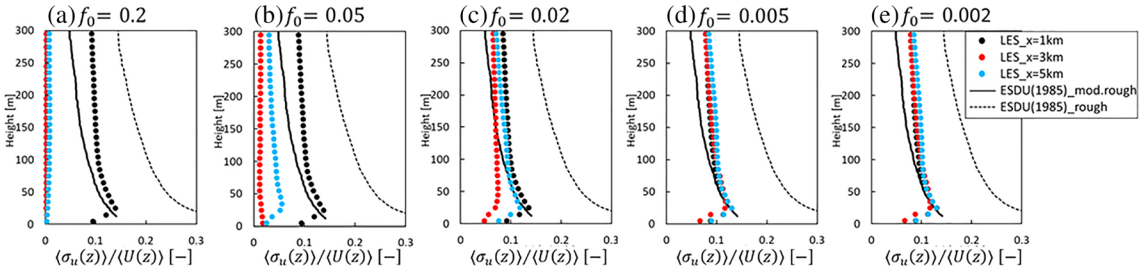

Figure 9. Vertical profiles of streamwise turbulence intensity for the cases of (a) $f_0 = 0.2$ s^{-1}, (b) $f_0 = 0.05$ s^{-1}, (c) $f_0 = 0.02$ s^{-1}, (d) $f_0 = 0.005$ s^{-1}, and (e) $f_0 = 0.002$ s^{-1}.

downstream position. This indicates that there are no significant differences among the data-assimilated LES results with different f_0 values and the equilibrium states of the TBL flow are maintained well throughout the computational region.

It is found from the sensitivity experiments that for f_0 %3E f_{peak}, the mean wind profile matches with the target one at the nudging area. However, the turbulent fluctuations are rapidly damped at downstream positions from the nudging area. For $f_0 \fallingdotseq f_{\mathrm{peak}}$, the mean wind velocity profile becomes similar to the target one. The turbulence intensities especially for the streamwise component are damped at the nudging area although those recover at $x = 5$ km. These results indicate that the equilibrium states of the TBL flow are not maintained. On the other hand, for f_0 %3C f_{peak}, the mean wind profile can be reasonably nudged toward the target one at the nudging area and maintain the equilibrium states of the TBL flows well throughout the computational region. This indicates that f_0 should be smaller than the f_{peak} of the background turbulence in order to nudge toward the target mean winds while maintaining the turbulent fluctuations well at short timescales of the order of 10 min.

5. Application to the Realistic Atmospheric Conditions

5.1. Meteorological Observations in the Urban Area of Kyoto

As an application to a real case, we used the meteorological observations conducted at the Ujigawa Open Laboratory of the Disaster Prevention Research Institute, Kyoto University, during the period from 12 January to 12 February 2016 (Yoshida et al., 2018). The laboratory is located in the southern part of Kyoto, Japan, which is composed of low-rise buildings and structures. The location of the observation site includes a 55 m high meteorological observation tower. A sonic anemometer (DA-600, Kaijo Co.) was installed on the tower at a 25-m height and measured three components of wind velocities and air temperature at a 10-Hz sampling rate. A Doppler lidar (WINDCUBE WLS-7, Leosphere) was also installed at the ground near the tower and measured three components of wind velocities at heights from 40 to 200 m with a 20-m interval at a sampling rate of 1 Hz. The conical scan angle is about 15.0°. Yoshida et al. (2018) extracted northerly, neutral conditions from the observations and chose the following four 30-min periods: 0720–0750 LT (local time = UTC + 9 h) 22 January; 1650–1720 LT 30 January; 0740–0810 LT 2 February; and

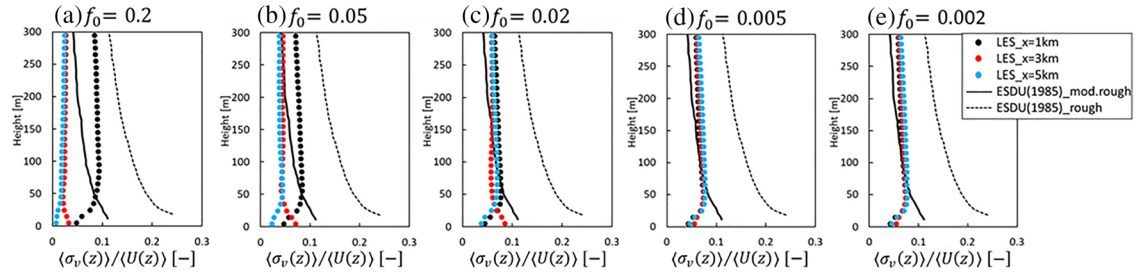

Figure 10. Vertical profiles of spanwise turbulence intensity for the cases of (a) $f_0 = 0.2$ s^{-1}, (b) $f_0 = 0.05$ s^{-1}, (c) $f_0 = 0.02$ s^{-1}, (d) $f_0 = 0.005$ s^{-1}, and (e) $f_0 = 0.002$ s^{-1}.

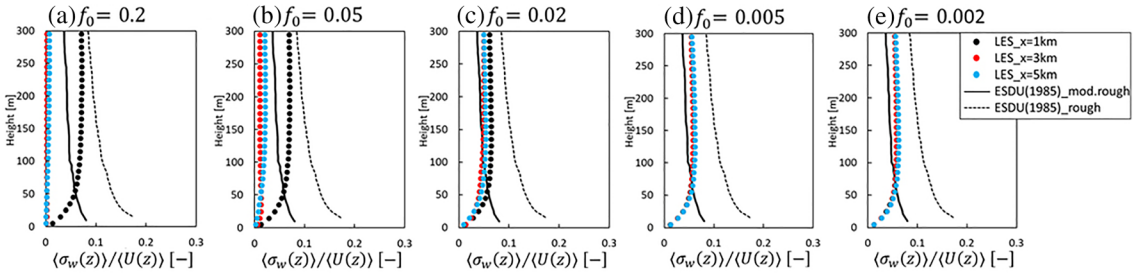

Figure 11. Vertical profiles of vertical turbulence intensity for the cases of (a) $f_0 = 0.2$ s^{-1}, (b) $f_0 = 0.05$ s^{-1}, (c) $f_0 = 0.02$ s^{-1}, (d) $f_0 = 0.005$ s^{-1}, and (e) $f_0 = 0.002$ s^{-1}.

1830–1900 LT 10 February. This study also used the data obtained during these time periods which are referred to as the D1, D2, D3, and D4 periods, respectively.

5.2. Computational Conditions

We used the same computational models as the ones described in section 3 and prescribed the observation site at 3 km downstream position from the inlet boundary in the analysis region. In order to focus on the influence of the data assimilation using the OBS data on turbulence structures, the building effects are represented by roughness length approach. The averaging building height (h_{av}) and roughness density (λ_f) of the urban area of Kyoto were estimated 9.8 m and 0.16 [−], respectively (Yoshida et al., 2018). Therefore, z_0 and u_* were set to 1.5 m and 0.4 m/s in Equation 8 based on Raupach's curve of z_0/h_{av} against λ_f (Raupach et al., 1980).

Figure 13 shows the vertical profiles of the mean wind speeds measured by the Doppler lidar and the input data for the data assimilation. Since the spatial resolution of the observed data was limited, the observed data were linearly interpolated on the vertical grids of the LES model. Below the 40-m height, the input data were given under the assumption of a mean wind vertical profile with $n = 0.25$. Above the 200-m height, those were given by the wind velocity data of the basic TBL flow. Since the OBS mean wind velocities for the D2 case are much larger than those for the other cases, the input data used for data assimilation in this case are nearly uniform in the vertical between the heights of 100–200 m. These input data were set uniformly for the spanwise direction at 3 km downstream positions from the inlet boundary in the analysis region.

5.3. LES Results by the Data Assimilation Method

We attempted to nudge the basic TBL flows toward the OBS data measured by the Doppler lidar by the data assimilation method using the vibration equation. Based on the sensitivity experiments as discussed in section 4, we prescribed $f_0 = 0.002$ in the vibration equation. Figure 14 shows instantaneous wind fields by the data assimilation method using the OBS data for the four cases. It is found that the wind velocities are actively fluctuating throughout the computational regions for each case. Figure 15 shows the vertical profiles of the 30-min averaged wind velocities. Those are also spatially averaged for the spanwise directions. For each case, the LES data are found to become close to the target OBS data at the nudging area. In particular, for the case of D2, the LES data are consistent with the target data. It seems that the LES data are

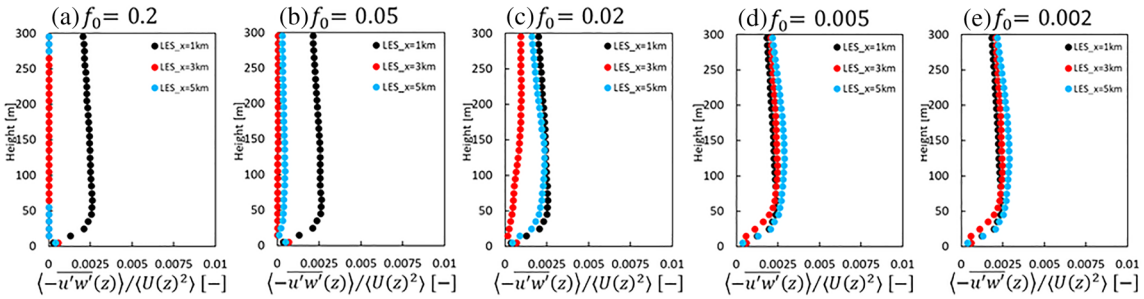

Figure 12. Vertical profiles of the Reynolds stress for the cases of (a) $f_0 = 0.2$ s^{-1}, (b) $f_0 = 0.05$ s^{-1}, (c) $f_0 = 0.02$ s^{-1}, (d) $f_0 = 0.005$ s^{-1}, and (e) $f_0 = 0.002$ s^{-1}.

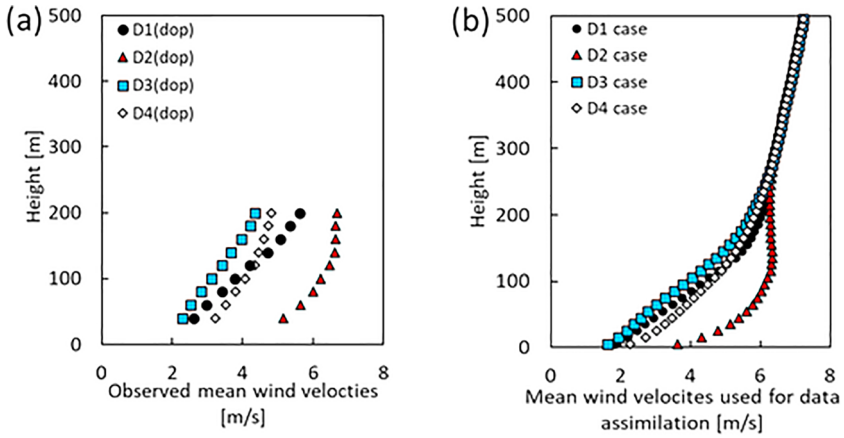

Figure 13. Vertical profiles of (a) meteorological observed data and (b) input data of mean wind velocities used for data assimilation. D1–4 indicate four 30-min periods: 0720–0750 JST 22 January, 1650–1720 JST 30 January, 0740–0810 JST 2 February, and 1830–1900 JST 10 February, respectively.

completely nudged toward the target OBS data for the case that the background mean winds are smaller than the target ones. The cause of this tendency should be further investigated. For all the cases, those at a downwind position from the nudging area of $x = 5$ km return to the original profile at $x = 1$ km.

Figures 16–18 show the vertical profiles of the streamwise, spanwise, and vertical turbulence intensities for each case. The streamwise and spanwise turbulence intensities measured by the Doppler lidar are much larger than the LES data and the upper limits of the ESDU. This is due to an overestimating bias for the

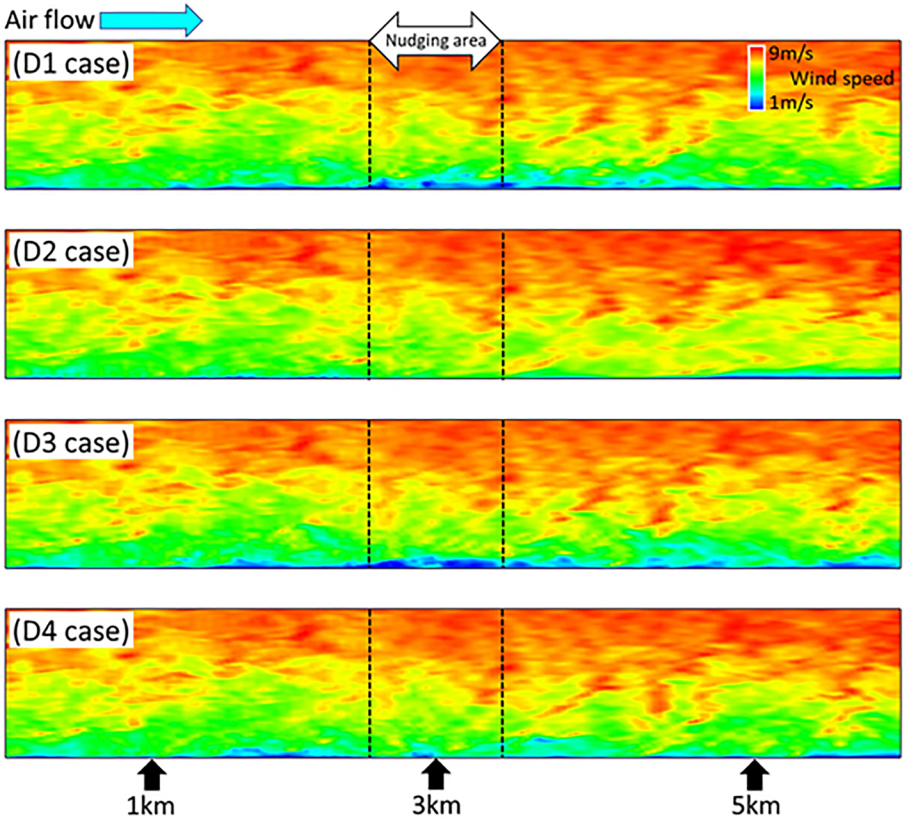

Figure 14. Instantaneous fields of wind speeds by the data assimilation method using the OBS data.

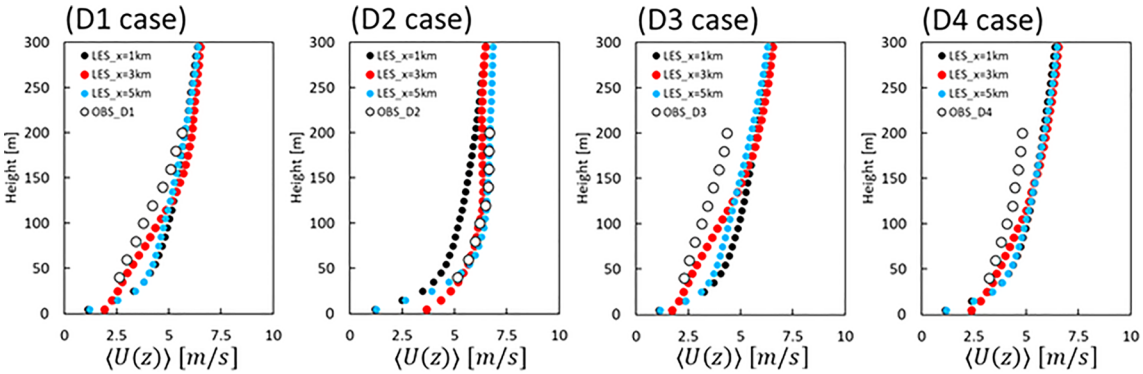

Figure 15. Vertical profiles of mean wind velocities for each case.

turbulence intensities (Yoshida et al., 2018). Since the turbulence intensities are mainly produced by the spatial gradient in mean wind velocity ($\partial U/\partial z$), those are sensitively influenced by the vertical profile pattern of the input data used for data assimilation. For the cases of D1 and D3, the streamwise turbulence intensities gently increase at heights from 50 to 150 m and slightly decrease at heights greater than 150 m at $x = 3$ km. In particular, for the case of D2, those are decreased by more than 20% above the 50-m height at $x \geq 3$ km. This is because the vertical profile of the input data used for data assimilation is nearly homogeneous for the vertical direction and the turbulent fluctuations are not actively generated. For the case of D4, the three components of the turbulence intensities at each downstream position are similar to one another. However, all the data for each component of the turbulence intensities generally lie in the range of the ESDU data for moderately rough and rough surfaces.

Figure 19 compares the vertical profiles of the simulated Reynolds stresses with the wind tunnel experimental data of Nosek et al. (2016) who generated a rough-wall TBL approximated with the power law of $n = 0.27$ by turbulence generators at the development section. The LES and experimental Reynolds stresses are normalized by the mean wind velocity at the 600-m height. We estimated the experimental data of the mean wind velocity at the 600-m height from the vertical profile of the 0.27 power law. The Reynolds stresses are sensitively influenced by the data assimilation. For the cases of D1, D3, and D4, those are increased at $x \geq 3$ km while those are decreased for the case of D2. According to the review by Counihan (1975) on adiabatic ABLs derived from the existing observational data, the normalized Reynolds stresses show the range from 0.0014 to 0.0043 for a moderately rough surface. The LES data are slightly underestimated in comparison with the data shown by Counihan (1975) at heights from 100 to 250 m for the case of D2. However, they generally lie in the range of the experimental data and the existing OBS data. It is shown from the data-assimilated LES results that the turbulence structures are sensitively influenced by the vertical distribution pattern of the OBS input data for data assimilation.

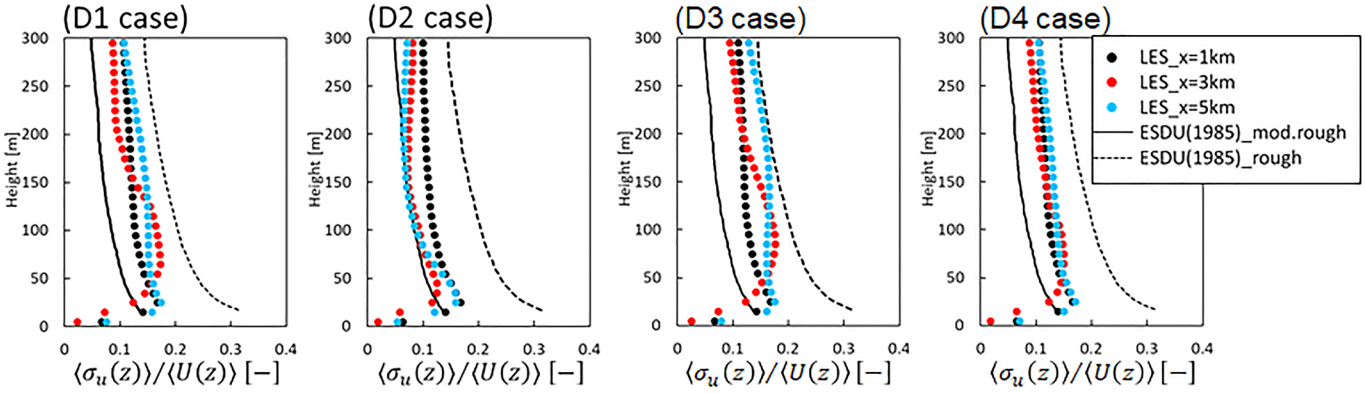

Figure 16. Vertical profiles of streamwise turbulence intensity for each case.

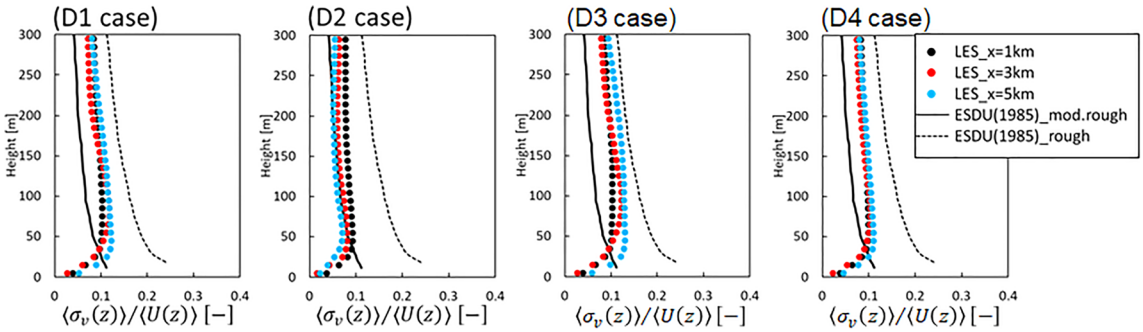

Figure 17. Vertical profiles of spanwise turbulence intensity for each case.

Pendergrass and Arya (1975a, 1975b) conducted wind tunnel experiments of the influence of turbulence intensities on the difference in plume dispersion for surface releases over smooth and rough surfaces. In their experiments, the streamwise and vertical turbulence intensities and Reynolds stresses over the rough surface were about 40%, 30%, and 50% greater than those over the smooth surface within the TBL, respectively. These differences in the turbulence structures induced the significant differences in the dispersion field. It was shown that the ratio between the respective maximum ground-level concentrations varies from 1.5 to 3, depending on stack height, and vertical and spanwise plume spreads are significantly different. These facts imply that differences of 30–40% in turbulence intensities of the TBL flows produce significant differences in plume dispersion behaviors. The application to LESs of plume dispersion needs to be made with caution. It is also important to discuss the influence of grid resolution on the data-assimilated LES results. Lu and Porte-Agel (2010) conducted a series of LESs with varying grid resolutions for a neutral ABL. They showed that the coarser resolution leads to a steep decrease of the power spectrum only at the high-frequency side due to the excessive dissipation. This implies that the dependency of grid resolution is small in the data assimilation method using a vibration equation since the spectral peak is not sensitive to it.

Although a critical issue remains in maintaining the equilibrium states of the TBL flows irrespective of input conditions used for data assimilation, the data-assimilated LES results of the turbulence intensities and Reynolds stresses are generally distributed around the vertical profiles of the empirical formulas and the wind tunnel experimental data. Therefore, it can be concluded that our proposed data assimilation method using the vibration equation successfully nudges toward the target mean winds while reasonably retaining the turbulent fluctuations. The successful representations of both mean and fluctuating winds are due to the idea to emphasize the oscillation term by neglecting the damping term in the vibration equation. The oscillation term is capable of both nudging the flow fields toward a target state and retaining the fluctuating nature of turbulent flows. With the oscillation terms, the turbulence statistics such as Reynolds stress and turbulent intensity can be favorably maintained.

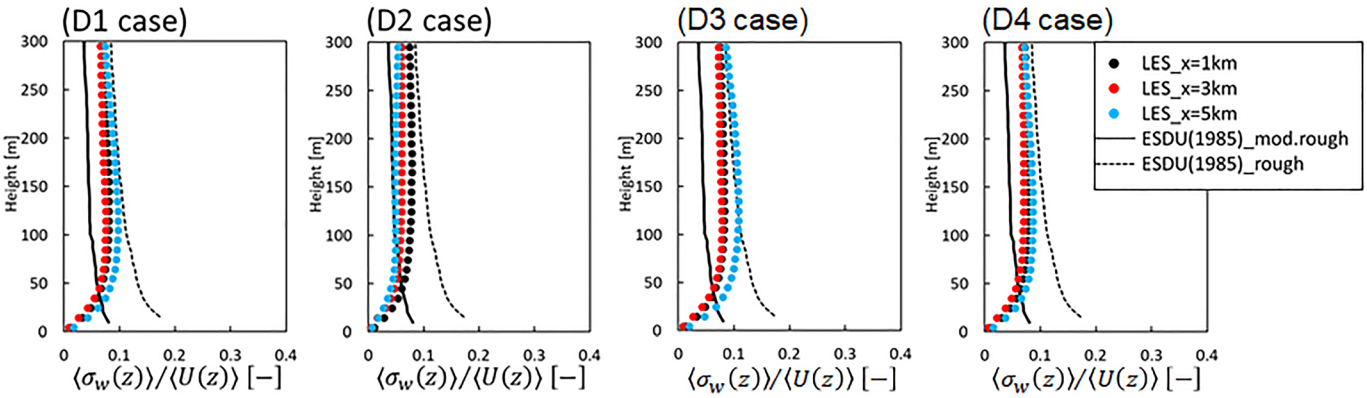

Figure 18. Vertical profiles of vertical turbulence intensity for each case.

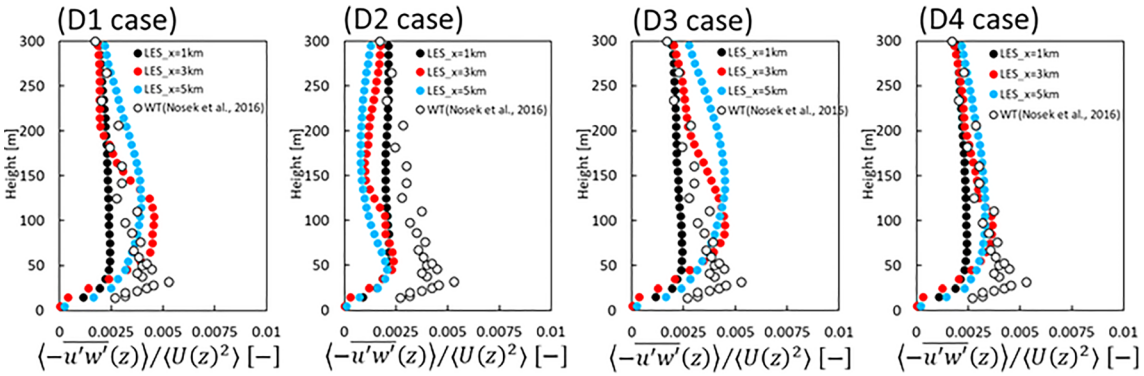

Figure 19. Vertical profiles of Reynolds stress for each case. The open circle depicts the wind tunnel experimental data (Nosek et al., 2016).

6. Conclusion

In this study, we proposed a data assimilation method using a vibration equation in order to nudge the LES-generated turbulence winds toward the target mean winds while maintaining the turbulent fluctuations. First, we conducted test simulations in which nudging is applied in a basic TBL flow toward a target one by prescribing a constant natural frequency value for the vertical direction and investigated an appropriate value for the natural frequency by conducting a number of sensitivity experiments. It is found that for a case of the natural frequency larger than the spectral peak one of the background turbulence, the turbulent fluctuations are rapidly damped at downstream positions from the nudging area although the mean wind profile matches with the target one at the nudging area. On the other hand, for a case of the natural frequency smaller than the spectral peak one of the background turbulence, the mean wind profile is reasonably nudged toward the target one at the nudging area while maintaining the turbulent fluctuations well. This indicates that the equilibrium states of the TBL flows are maintained well. The sensitivity experiments show that the natural frequency should be smaller than the spectral peak one of the background turbulence in order to nudge toward the target mean winds while maintaining the turbulent fluctuations at short timescales of the order of 10 min. It was also found that there are no significant differences among the data-assimilated LES results of mean velocities, turbulence intensities, and Reynolds stresses with the different natural frequency values under the condition of the natural frequency smaller than the spectral peak one of the background turbulence. It is practically preferred to impose much smaller constant natural frequency value for the vertical direction than the peak frequency.

Then, we applied the proposed nudging method by incorporating data obtained from meteorological observations located in the southern part of the actual city of Kyoto. The mean wind velocity profiles were reasonably nudged toward the target observed profile. However, it was found that the data-assimilated LES results of the turbulence structures were sensitively influenced by the vertical distribution pattern of the input data used for data assimilation. There was a tendency to decrease the turbulence intensities by 20–30% when the vertical profile of the input data was nearly homogeneous. Such a decrease in the turbulence intensities could produce significant errors in predicting plume dispersion behaviors. Although a critical issue remains in maintaining the equilibrium states of the TBL flows irrespective of input conditions used for data assimilation, it was shown that the turbulence statistics such as Reynolds stress and turbulent intensity are favorably retained in comparison with the empirical formulas and experimental data. These facts indicate that the oscillation term, by neglecting the damping term in the vibration equation, is capable of both nudging the flow fields toward a target state and retaining the fluctuating nature of turbulent flows. It is concluded that our proposed data assimilation method is suitable for LES models and has a high potential to practically reproduce more realistic atmospheric state.

In future work, we apply the data assimilation method to MMS-CFD coupling simulations for the field campaign Joint Urban 2003 conducted in the urban central district of Oklahoma City. In this field campaign, the meteorological observations were conducted at several sites in and around the urban central district. We need to conduct building-resolving CFD simulations of plume dispersion in the complex urban environments and investigate the effectiveness of our data assimilation technique in comparison with the field experimental data of wind velocities and concentrations.

Data Availability Statement

All the data used in this study are stored in a repository, accessible through this link (DOI: 10.5281/zenodo.3872449; https://zenodo.org/record/3872449).

Acknowledgments
This work was supported by JSPS KAKENHI grant JP18H01680. The LESs were performed on the ICEX at Japan Atomic Energy Agency.

References

Beare, R. J., Cortes, M. A. J., Cuxart, J., Esau, I., Golaz, C., Holtslag, A. A. M., et al. (2006). An intercomparison of large-eddy simulations of the stable boundary layer. *Boundary-Layer Meteorology*, *118*(2), 247–272. https://doi.org/10.1007/s10546-004-2820-6

Cheng, H., & Castro, I. P. (2002). Near wall flow over urban-like roughness. *Boundary-Layer Meteorology*, *104*(2), 229–259. https://doi.org/10.1023/A:1016060103448

Counihan, J. (1975). Adiabatic atmospheric boundary layers: A review and analysis of data from the period 1880–1972. *Atmospheric Environment*, *9*(10), 871–905. https://doi.org/10.1016/0004-6981(75)90088-8

Dudhia, J. (1993). A nonhydrostatic version of the Penn State/NCAR mesoscale model: Validation tests and simulation of an Atlantic cyclone and cold front. *Monthly Weather Review*, *121*(5), 1493–1513. https://doi.org/10.1175/1520+0493(1993)121%3C1493:ANVOTP%3E2.0.CO;2

Dupont, S., Bonnefond, J., Irvine, M., Lamaud, E., & Brunet, Y. (2011). Long-distance edge effects in a pine forest with a deep and sparse trunk space: In situ and numerical experiments. *Agricultural and Forest Meteorology*, *151*(3), 328–344. https://doi.org/10.1016/j.agrformet.2010.11.007

Germano, M., Piomelli, U., Moin, P., & Cabot, W. H. (1991). A dynamic subgrid-scale eddy viscosity model. *Physics of Fluids*, *A3*(7), 1760–1765.

Harlow, F., & Welch, J. E. (1965). Numerical calculation of time-dependent viscous incompressible flow of fluid with a free surface. *Physics of Fluids*, *8*(12), 2182–2189. https://doi.org/10.1063/1.1761178

Heinze, R., Moseley, C., Böske, L., Muppa, S., Maurer, V., Raasch, S., & Stevens, B. (2017). Evaluation of large-eddy simulations forced with mesoscale model output for a multi-week period during a measurement campaign. *Atmospheric Chemistry and Physics*, *17*(11), 7083–7109. https://doi.org/10.5194/acp-17-7083-2017

Iizuka, S., & Kondo, H. (2004). Performance of various sub-grid scale models in large-eddy simulations of turbulent flow over complex terrain. *Atmospheric Environment*, *38*(40), 7083–7091. https://doi.org/10.1016/j.atmosenv.2003.12.050

Kanda, M. (2006). Large-eddy simulations on the effects of surface geometry of building arrays on turbulent organized structures. *Boundary-Layer Meteorology*, *118*(1), 151–168. https://doi.org/10.1007/s10546-005-5294-2

Kanda, M., Inagaki, A., Miyamoto, T., Gryschka, M., & Raasch, S. (2013). A new aerodynamic parameterization for real urban surfaces. *Boundary-Layer Meteorology*, *148*(2), 357–377. https://doi.org/10.1007/s10546-013-9818-x

Keating, A., Prisco, G., & Piomelli, U. (2006). Interface conditions for hybrid RANS/LES calculations. *International Journal of Heat and Fluid Flow*, *27*(5), 777–788. https://doi.org/10.1016/j.ijheatfluidflow.2006.03.007

Laraufie, R., Deck, S., & Sagaut, P. (2011). A dynamic forcing method for unsteady turbulent inflow conditions. *Journal of Computational Physics*, *230*(23), 8647–8663. https://doi.org/10.1016/j.jcp.2011.08.012

Lu, H., & Porte-Agel, F. (2010). A modulated gradient model for large-eddy simulation: Application to a neutral atmospheric boundary layer. *Physics of Fluids*, *22*(1), 015109. https://doi.org/10.1063/1.3291073

Maronga, B., Gryschka, M., Heinze, R., Hoffmann, F., Kanani-Sühring, F., Keck, M., et al. (2015). The Parallelized Large-Eddy Simulation Model (PALM) version 4.0 for atmospheric and oceanic flows: Model formulation, recent developments, and future perspectives. *Geoscientific Model Development*, *8*(8), 2515–2551. https://doi.org/10.5194/gmd-8-2515-2015

Moin, P., & Kim, J. (1982). Numerical investigation of turbulent channel flow. *Journal of Fluid Mechanics*, *118*(1), 341–377. https://doi.org/10.1017/S0022112082001116

Monin, A., & Obukhov, M. (1954). Basic laws of turbulent mixing in the ground layer of the atmosphere. *Trudy Akademii Nauk SSSR Geophiz Institute*, *24*, 163–187.

Nakayama, H., Leitl, B., Harms, F., & Nagai, H. (2014). Development of local-scale high-resolution atmospheric dispersion model using large-eddy simulation part 4: Turbulent flows and plume dispersion in an actual urban area. *Journal of Nuclear Science and Technology*, *51*(5), 626–638. https://doi.org/10.1080/00223131.2014.885400

Nakayama, H., Takemi, T., & Nagai, H. (2012). Large-eddy simulation of urban boundary-layer flows by generating turbulent inflows from mesoscale meteorological simulations. *Atmospheric Science Letters*, *13*(3), 180–186. https://doi.org/10.1002/asl.377

Nakayama, H., Takemi, T., & Nagai, H. (2016). Development of local-scale high-resolution atmospheric dispersion model using large-eddy simulation part 5: Detailed simulation of turbulent flows and plume dispersion in an actual urban area under real meteorological conditions. *Journal of Nuclear Science Technology*, *53*(6), 887–908. https://doi.org/10.1080/00223131.2015.1078262

Neggers, R. A. J., Siebesma, A. P., & Heus, A. T. (2012). Continuous single-column model evaluation at a permanent meteorological supersite. *Bulletin of the American Meteorological Society*, *93*(9), 1389–1400. https://doi.org/10.1175/BAMS-D-11-00162.1

Nosek, S., Kukacka, L., Kellnerova, R., Jurcakova, K., & Janour, Z. (2016). Ventilation processes in a three-dimensional street canyon. *Boundary-Layer Meteorology*, *159*(2), 259–284. https://doi.org/10.1007/s10546-016-0132-2

Pendergrass, W., & Arya, S. P. S. (1975a). Dispersion in neutral boundary layer over a step change in surface roughness—I. Mean flow and turbulence structure. *Atmospheric Environment*, *18*, 1267–1279.

Pendergrass, W., & Arya, S. P. S. (1975b). Dispersion in neutral boundary layer over a step change in surface roughness—II. Concentration profiles and dispersion parameters. *Atmospheric Environment*, *18*, 1281–1296.

Raupach, M. R., Thom, A. S., & Edwards, I. (1980). A wind tunnel study of turbulent flow close to regularly arrayed rough surfaces. *Boundary-Layer Meteorology*, *18*(4), 373–397. https://doi.org/10.1007/BF00119495

Santiago, J. L., Coceal, O., Martilli, A., & Belcher, S. E. (2008). Variation of the sectional drag coefficient of a group of buildings with packing density. *Boundary-Layer Meteorology*, *128*(3), 445–457. https://doi.org/10.1007/s10546-008-9294-x

Skamarock, W. C., Klemp, J. B., Dudhia, J., Gill, D. O., Barker, D. M., Duda, M. G., et al. (2008). A description of the Advanced Research WRF version 3. NCAR Tech. Note, NCAR/TN-47 + STR, p. 113.

Smagorinsky, J. (1963). General circulation experiments with the primitive equations. *Monthly Weather Review*, *91*(3), 99–164. https://doi.org/10.1175/1520-0493(1963)091%3C0099:GCEWTP%3E2.3.CO;2

Spille-Kohoff, A. & KaltenBach, H. (2001). Generation of turbulent inflow data with a prescribed shear-stress profile, DNS/LES Progress and Challenges, Third AFOSR International Conference, Arlington, Texas, 319-326.

Warner, S., Platt, N., & Heagy, J. F. (2004). Comparison of transport and dispersion model predictions of the URBAN 200 field experiment. *Journal of Applied Meteorology*, *43*(6), 829–846. https://doi.org/10.1175/1520-0450(2004)043%3C0829:COTADM%3E2.0.CO;2

Xie, Z. T., & Castro, I. P. (2006). LES and RANS for turbulent flow over arrays of wall-mounted obstacles. *Flow, Turbulence and Combustion*, *76*(3), 291–312. https://doi.org/10.1007/s10494-006-9018-6

Yoshida, T., Takemi, T., & Horiguchi, M. (2018). Large-eddy-simulation study of the effects of building-height variability on turbulent flows over an actual urban area. *Boundary-Layer Meteorology*, *168*(1), 127–153. https://doi.org/10.1007/s10546-018-0344-8